JOURNAL OF EXPERIMENTAL AND THEORETICAL PHYSICS, 2024, Vol. 165, No. 1, pp. 84–92

SOLIDS AND LIQUIDS

ENERGY SPECTRUM AND OPTICAL ABSORPTION OF C_{50} AND C_{70} FULLERENE COMPOUNDS WITH Cl AND Br ATOMS

© 2024 A. I. Murzashev*, A. P. Zhumanazarov

Mari State University, Faculty of Physics and Mathematics

Yoshkar-Ola, 424000, Russia

*e-mail: nanotubes59@mail.ru

Received September 05, 2023

Revised September 21, 2023

Accepted September 21, 2023

Abstract. Within the framework of the static fluctuation approximation for the Hubbard model, the energy spectrum and optical absorption spectrum of the compounds $C_{50}Cl_{10}$ and $C_{70}Br_{10}$ were calculated. Optical absorption spectra of the studied systems, calculated taking into account the fact that carbon at the attachment sites of chlorine or bromine atoms passes from the sp^2 hybridized state to the sp^3 hybridized state. The curves of the optical absorption spectrum obtained within the framework of the proposed model are in qualitative agreement with experimental data.

Keywords: *energy spectrum, optical absorption, strong Coulomb interaction, The Hubbard model, strong related state, Hubbard's sub zones, Green's two-particle functions*

DOI: 10.31857/S00444510240109e5

1. INTRODUCTION

The researchers' interest in studying fullerene-based compounds is to a certain extent related to the search for new compounds, candidates for the basic element base for micro- and nanoelectronics. This interest is also supported by the development of molecular design methods [1]. In this regard, endohedral fullerenes are primarily of interest. These compounds are fullerene with a metal atom inside its carbon shell. The electronic structure of such systems can be described with good accuracy as an electronic subsystem of pure, free fullerene without impurities, to the vacant energy levels of which excess electrons are added: valence electrons of the metal atom. Thus, the valence electrons of this metal atom pass into the π-electronic fullerene subsystem.

In addition, there has long been an interest in another type of fullerene-based compounds. By analogy with endohedral ones, it is convenient to call them exohedral fullerenes. In these compounds, the molecular atoms are located not inside the fullerene shell, but on its surface. Such primitive atoms, as a rule, are atoms of chemical elements of the halogen group, for example Cl, Br et al., as well as groups of atoms containing halogen atoms. A good example of such a group of atoms is the so-called trifluoromethyl CF_3 groups. Such atoms and groups of atoms are strong oxidizing agents, and their attachment to fullerene occurs by forming an ionic chemical bond. At the same time, from the fullerene node, to which an impurity atom is attached, π-electrons escape into the outer shell of this atom. In pure fullerene, all carbon atoms are in the hybridized sp^2 state, three of the four valence carbon atoms are involved in the formation of chemical bonds (σ bonds) with neighboring atoms, and the fourth (non-hybrid) electron forms the π zone. Obviously, in the attachment node when a chemical bond is formed with an attached atom, a fourth electron is also involved, which previously belonged to the π-subsystem. As a result, carbon in the attachment site will no longer be in the sp^2-, but in the hybridized sp^3-state. Obviously, as a result of this, the π-electron subsystem of fullerene loses not only the π-electron, but also the node on which it can be located. The above is supported by the results of the work [2], according to which NMR studies show the presence of carbon in the $C_{50}Cl_{10}$ system indicated not only in the sp^2-state, but also in the sp^3-state.

In a number of our works, for example in [3–5], it was shown that all the electronic and optical properties of fullerenes are almost completely determined by the π-electron subsystem. Then it is obvious that these properties in the compounds described above will depend significantly on both the number of attached halogen atoms (or groups of atoms) and their distribution over the fullerene surface. This

was convincingly shown by us in [6, 7] using the example of compounds $C_{60}(CF_3)_{10}$, $C_{70}(CF_3)_{10}$ and $C_{90}Cl_n$. The calculations in [6, 7] were performed in the approximation of static fluctuations for the Hubbard model, described in detail in a number of our works, for example, [3–5, 8–10]. However, unlike pure or endohedral fullerenes in [6, 7], we modified the approximation used in [3–5, 8–10]. Taking into account the fact that in the nodes of the connection of the systems $C_{60}(CF_3)_{10}$, $C_{70}(CF_3)_{10}$ and $C_{90}Cl_n$ carbon is not in the sp^2-, but in the sp^3-state, the energy spectrum of the π-electron subsystem was calculated with the exclusion of nodes with sp^3 hybridization. Thus, the present work is devoted to the calculation of the energy spectrum and the optical absorption spectrum of the compounds $C_{50}Cl_{10}$ and $C_{70}Br_{10}$. The first compound was synthesized and studied in [2, 11], the second in [12]. It should be said here that there are two papers [13, 14] in which an attempt was made to calculate the energy spectrum of $C_{50}Cl_{10}$ systems and $C_{70}Br_{10}$; in our opinion, the results obtained in these studies are incorrect, since their preparation does not take into account the fact that carbon in the attachment nodes is not in the sp^2-, but in the sp^3-state.

2. MODEL AND METHOD

It is known that in carbon systems with sp^2 hybridization, the intra-node Coulomb interaction is large and can reach values of about 10 eV [15,16]. Systems with the same values of the Coulomb integral can be described most correctly in the framework of the Hubbard model [17]. The Hamiltonian of this model can be written as follows:

$$H = \varepsilon\sum_{i,\sigma}\hat{n}_{i,\sigma} + B\sum_{i,j,\sigma}\left(a^{\dagger}_{i,\sigma}a_{j,\sigma} + a^{\dagger}_{j,\sigma}a_{i,\sigma}\right) + U\sum_{i}\hat{n}_{i\uparrow}\hat{n}_{i\downarrow}. \quad (1)$$

Here, the first term describes the intrinsic energy of the π-electrons, the second one takes into account the jumps of electrons from node to node, and the third the Coulomb interaction of electrons at one node. The variables ε, B and U denote the intrinsic energy of the electrons, the leap integral and the Coulomb interaction integral, respectively. Finally, $\hat{n}_{i,\sigma} = a^{\dagger}_{i,\sigma}, a_{i,\sigma}$ is the operator of the number of particles in node i with spin σ, and $a^{\dagger}_{i,\sigma}, a_{i,\sigma}$ are the operators of the generation and destruction of electrons with spin σ at the i-th node, respectively. In (1) summation according to i, is performed on all atoms of the system, and in the second term on the nodes j adjacent to the nodes i. Despite the simple and understandable form of the Hamiltonian, the task of finding the energy spectrum systems with such a Hamiltonian are extremely complex. The existing approximate methods work only in the limit when the integral of the Coulomb interaction is $U \gg W$, W is the width of the conduction band. Obviously, these methods are not applicable for carbon systems with sp^2 hybridization, since according to [18] $W = 6|B|$, the Coulomb integral, taking into account the shielding is $U \approx 7.0$ eV [16], $B \approx -1.0$ eV [3].

In [3, 4, 19], we used the static fluctuations approximation (SFA) to find the energy spectrum of fullerene and carbon nanotubes. In short, the essence of the SFA is as follows: for the birth operator $a^{\dagger}_{i\sigma}$, taken in the Heisenberg representation with Matsubara time τ, we write down the equations of motion. After simple transformations, we obtain

$$\frac{da^{\dagger}_{f\sigma}(\tau)}{d\tau} = \varepsilon_{f\sigma}a^{\dagger}_{f\sigma}(\tau) + B\sum_{j\neq f}a^{\dagger}_{j\sigma}(\tau) + Ua^{\dagger}_{f\sigma}(\tau)\Delta n_{f\bar{\sigma}}(\tau). \quad (2)$$

Here $\varepsilon_{f\sigma} = \varepsilon + U\langle n_{f\bar{\sigma}}\rangle$, $\bar{\sigma}$ denotes the projection of the electron spin opposite σ, $\langle n_{f\bar{\sigma}}\rangle$ is the average value of the operator $\hat{n}_{f\bar{\sigma}}$, $\Delta n_{f\bar{\sigma}}, \hat{n}_{f\bar{\sigma}} = \langle n_{f\bar{\sigma}}\rangle$. By entering operators $\tilde{a}^{\dagger}_{f\bar{\sigma}}(\tau)$ using the representation

$$a^{\dagger}_{i\sigma}(\tau) = \exp(H_0\tau)\tilde{a}^{\dagger}_{i\sigma}(\tau)\exp(-H_0\tau), \quad (3)$$

where

$$H_0 = \sum_{i,\sigma}\varepsilon_{i\sigma}n_{i,\sigma} + B\sum_{i,j,\sigma}\left(a^{\dagger}_{i,\sigma}a_{j,\sigma} + a^{\dagger}_{j,\sigma}a_{i,\sigma}\right),$$

after simple calculations, assuming that $[H_0, H] \approx 0$, for the birth operator in the Heisenberg representation, we obtain the following expression:

$$a^{\dagger}_{k\sigma}(\tau) = \bar{a}^{\dagger}_{k\sigma}(\tau)\frac{1}{2}\left(e^{\frac{U}{2}\tau} + e^{-\frac{U}{2}\tau}\right). \quad (4)$$

The designation is introduced here

$$\bar{a}^{\dagger}_{k\sigma}(\tau) = e^{H_0\tau}a^{\dagger}_{k\sigma}(0)e^{-H_0\tau}.$$

In other words, to find $a^{\dagger}_{i,\sigma}(\tau)$ it is necessary to find $\bar{a}^{\dagger}_{i,\sigma}(\tau)$. To find $\bar{a}^{\dagger}_{i,\sigma}(\tau)$ we write down the equations of motion:

$$\frac{d\bar{a}^{\dagger}_{k\sigma}(\tau)}{d\tau} = \varepsilon_k\bar{a}^{\dagger}_{k\sigma}(\tau) + B\sum_{j\neq k}\bar{a}^{\dagger}_{j\sigma}(\tau). \quad (5)$$

Thus, in order to find the operators in the Heisenberg representation, it is necessary to solve (5) a system of linear

differential equations. When applied to a specific fullerene, the number of equations in the system is equal to the number of fullerene nodes. Having solved (5), we find $\overline{a}^{\dagger}_{k\sigma}(\tau)$ and using (4) we find the birth operators in the Heisenberg representation of $a^{\dagger}_{k\sigma}(\tau)$. Knowing these operators, we find the anticommutative Green functions

$$G_{k\sigma}(\tau) = \theta(\tau)\langle[a^{\dagger}_{k\sigma}(\tau), a_{k\sigma}(0)]_{+}\rangle \tag{6}$$

and correlation functions

$$\wp_{ik\sigma}(\tau) = \theta(\tau)\langle[a^{\dagger}_{i\sigma}(\tau), a_{k\sigma}(0)]_{+}\rangle. \tag{7}$$

Here the square brackets $[...]_{+}$ denote the anti-commutator, and $\theta(\tau)$ is a known discontinuous function equal to one for positive values of the argument and to zero for negative ones. Knowing Green's functions, one can find the energy spectrum of the system as the poles of the Fourier image summed over all nodes of Green's function. For each specific fullerene, the Green function summed up for all nodes will look like

$$G(\tau) = \sum_{k} M_k e^{E_k \tau}, \tag{8}$$

here E_k and M_k are the energy values of the level and the multiplicity of degeneracy of this level, respectively. It is clearly seen that all M_k have integer values and their sum is equal to the number of fullerene nodes.

An analysis of the results shows that the essence of the SFA is as follows: expression (4) is obtained with precise consideration of the intra-node Coulomb repulsion, while neglecting the electron jumps from node to node, and the system (5) accurately takes into account the processes of electron jump from node to node, while the intra-node Coulomb repulsion is neglected. Thus, the SFA accurately takes into account the two main processes in the system, but neglects the processes of their interference. Obviously, if the interference of these processes is "turned on", it will be necessary to take into account processes with electron spin flaps. These processes lead to the Kondo effect [20], to ferro- and antiferromagnetic ordering, to the competition of charge ordering and Cooper pairing (superconductivity) [21]. All these processes take place at low temperatures. That is, the scope of application of the SFA is room temperature.

The application of the described method in [3–5, 8–10] showed that the energy spectrum of fullerenes, taking into account the intra-node Coulomb interaction, divides the π-electronic subsystem into two groups of levels, the upper and lower Hubbard subzones. The states of the "lower" Hubbard subzone correspond to the states of electrons with a single occupation of the node, the" upper" with a double occupation of the node. The "lower" Hubbard subzone is completely filled, the "upper" one is completely vacant. In such systems, each energy level with the multiplicity of degeneracy M is already filled with non-M electrons with the spin "up" and M electrons with the spin "down", and M electrons with an arbitrary spin orientation.

The energy spectrum of fullerenes cannot be measured directly. It is more or less possible to measure the density of electronic states, which can be constructed from the calculated energy spectrum. Unfortunately, such experiments are complex and rarely found in literature. The most frequently measured characteristic of fullerenes is their optical absorption spectrum (OAS). Almost every work devoted to the synthesis of one or another fullerene, isomer shows the measured OAS curve.

In connection with the above, the task of finding the dependence of the intensity of absorption of electromagnetic radiation on its frequency is of great practical interest. Obviously, this characteristic is completely determined by the energy spectrum. Knowing the energy spectrum and fullerene symmetry, it is possible to find selection rules for transitions allowed between different energy levels. Assuming that the intensity of each transition does not depend on the energy levels E_k and E_i, the transition between which occurs with the absorption of a photon of energy $\hbar\omega$, using Fermi's rule [22], the absorption intensity can be found by the formula

$$\mathrm{In}(\hbar\omega) \sim \sum_{k,i} M_k M_i \frac{\delta}{(E_k - E_i - \hbar\omega)^2 + \delta^2}. \tag{9}$$

Here, δ is a phenomenological parameter that takes into account the attenuation of electronic states, M_k, M_i, the multiplicity of degeneracy of energy levels E_k and E_i, respectively. In (9), the summation is carried out for all transitions between filled and vacant levels, the transitions between which are regulated by the selection rules. In a number of papers [8, 23, 24], we used this method of finding the intensity of absorption. Despite the approximation of this formula, our OAS curves obtained by this method coincide with the experimental data at a good qualitative level.

A more accurate formula for finding the dependence of the absorption intensity on the frequency of absorbed

electromagnetic waves can be found if we use the Kubo formula, according to which the generalized susceptibility of the system can be written:

$$\sigma(\omega) = \text{const}\sum_{i,j,\sigma}\wp_{ik\sigma}(\tau)\wp_{ki\sigma}(\tau)\,|_{\omega}\,. \qquad (10)$$

Here $|_{\omega}$ means taking the Fourier image from the expression on the left. Within the framework of the SFA, expressions for correlation functions can be obtained $\wp_{ik\sigma}(\tau)$. For fullerenes, the expressions for these functions will have the form

$$\wp_{ik}(\tau) = \sum_{\alpha} W_{\alpha}^{(ik)} e^{E_{\alpha}^{(ik)}\tau}, \qquad (11)$$

where are $W_{\alpha}^{(ik)}$ numbers different for each particular system and each specific correlation function, and $E_{\alpha}^{(ik)}$ are the values of certain energy levels of the system under study. Considering that the imaginary part of the generalized susceptibility is responsible for absorption, for the optical absorption spectrum curve we obtain the following expression:

$$\text{Im}\chi(\omega) \sim \sum_{\alpha,\beta}\frac{W_{\alpha}^{(ik)}W_{\beta}^{(ki)}\left[n\left(E_{\alpha}^{(ik)}\right) - n\left(E_{\beta}^{(ki)}\right)\right]\delta}{\left(E_{\alpha}^{(ik)} - E_{\beta}^{(ki)} - \omega\right)^2 + \delta^2}. \qquad (12)$$

Here $n(x)$ is the Fermi distribution function, which in our case can be represented with great accuracy in the form

$$n(x) = \begin{cases}1, & x < 0,\\ 0, & x > 0,\end{cases} \qquad (13)$$

δ originally, in the theory of Green's functions [25], is an infinitesimal value that provides a correct choice of the integration contour, but in the case of specific systems, δ is a phenomenological parameter that takes into account the attenuation of the electronic states of an open system. It can be seen from (12) that the expression $[n(E_{\alpha}^{(ik)}) - n(E_{\beta}^{(ki)})]$ in the numerator ensures selection so that transitions occur only between filled and vacant states. The selection according to the states between which a transition is possible is determined by what terms are included in the expressions for correlation functions (11). The multipliers $W_{\alpha}^{(ik)}$ and $W_{\beta}^{(ki)}$ set the intensity of each acquisition line. The analysis of formula (12), which the authors continue to work on, indicates that (12) contains transitions, both permitted and prohibited by the selection rules. The first transitions lie in the short-wave region, the second, forbidden ones, in the long-wave region. This assertion, at that time still as a hypothesis, was put forward by us in [8, 26].

3. THE ENERGY SPECTRUM AND OPTICAL ABSORPTION OF $C_{50}Cl_{10}$ COMPOUND

In [2], the synthesis of the compound $C_{50}Cl_{10}$ is reported. The synthesis was carried out by the method of electro-arc discharge on carbon electrodes in a helium atmosphere with the addition of four carbon chloride atoms. In the work, it was found that the obtained compound belongs to the symmetry group D_{5h}, to which 10 chlorine atoms are attached according to the "equator", as shown in Fig. 1. The authors of [2] suggested that the synthesized compound, being smaller than that of C_{60}, should have unusual properties, which should be a consequence of the high curvature of the surface. However, due to the small amount of the synthesized compound, about 2 mg, it was not possible to make any measurements in [2]. Later, in almost 10 years, the compound $C_{50}Cl_{10}$ was investigated in more detail in [11]. The OAS of this compound, measured in this work, is shown in Fig. 2.

It can be seen that there are bands on the absorption curve with maxima of 238, 322, 334, 356 nm, and the absorption edge occurs at a wavelength of $\lambda \sim 450$ nm.

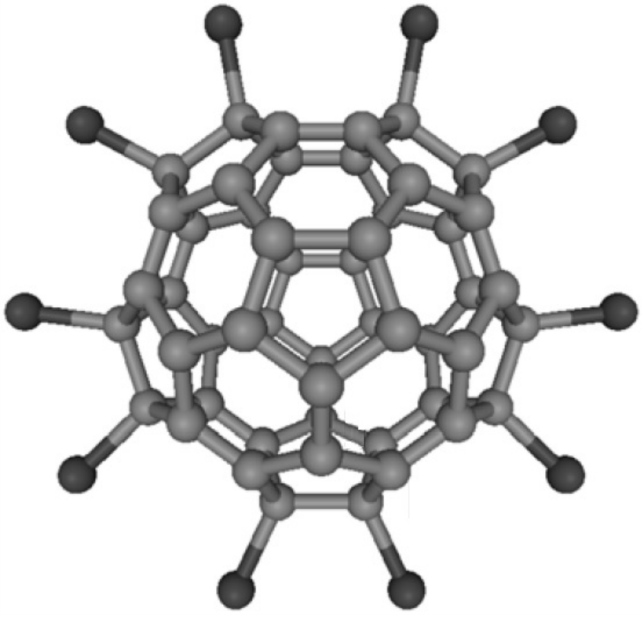

Fig. 1. Image of the $C_{50}Cl_{10}$ compound. Data from work [2] were used.

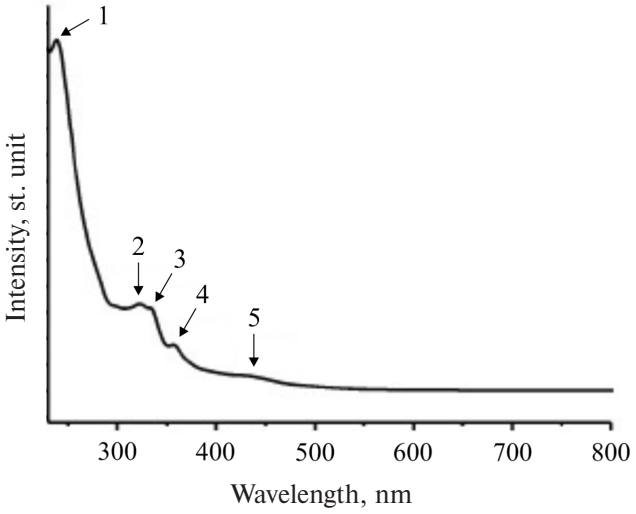

Fig. 2. Optical absorption spectrum of the compound $C_{50}Cl_{10}$. 1–238 nm, 2–322 nm, 3–334 nm, 4–356 nm, 5–434 nm. Data from [11] are used.

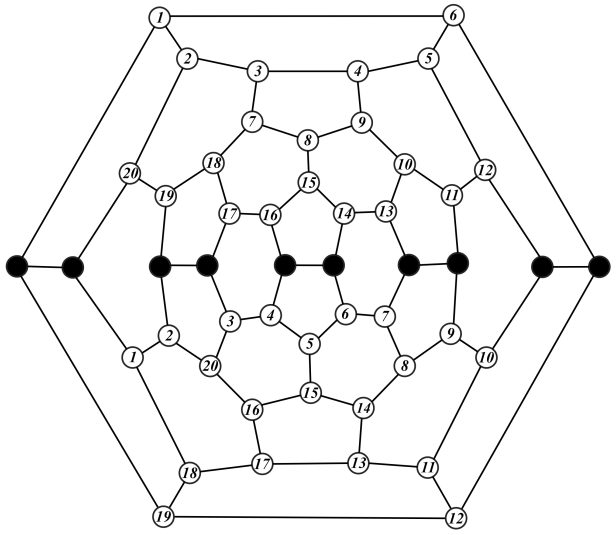

Fig. 3. The Schlegel diagram of the compound $C_{50}Cl_{10}$.

As mentioned above, at the attachment points of halogen atoms, carbon passes from the hybridized sp^2-state to the sp^3-state. As a result, these nodes must be removed from consideration. Fig. 3 shows the Schlegel diagram of the compound under study. In the figure, empty circles indicate nodes free of chlorine atoms, filled nodes through which chlorine atoms are attached. Due to the fact that at these nodes, carbon passes into a hybridized sp^3-state, the π-electron subsystem is divided into two subsystems, as shown in Fig. 4. It can be seen that chlorine atoms divide the studied compound into two equivalent subsystems.

Thus, to calculate the energy spectrum of the compound under study, it is necessary to calculate the energy spectrum of one of the "clusters". By the method described above for the system, the Schlegel diagram of which is shown in Fig. 4, the energy spectrum was calculated at the values of the parameters of the Hubbard model U = 8.1 eV and B = −1.0 eV. The values of the energy levels and the multiplicity of their degeneracy are given in Table 1.

In each cell of this table, the first number is the energy of the level in eV, the second is the multiplicity of the level degeneracy. Levels with negative energy values correspond to the filled states, with positive ones to vacant ones. The filled states belong to the lower Hubbard subzone, while the vacant ones belong to the "upper" Hubbard subzone. Each subzone contains 12 levels, of which 8 are two- fold degenerate, and 4 are single-fold. The width of each Hubbard subzone is approximately 5.14 eV, and the gap between the filled

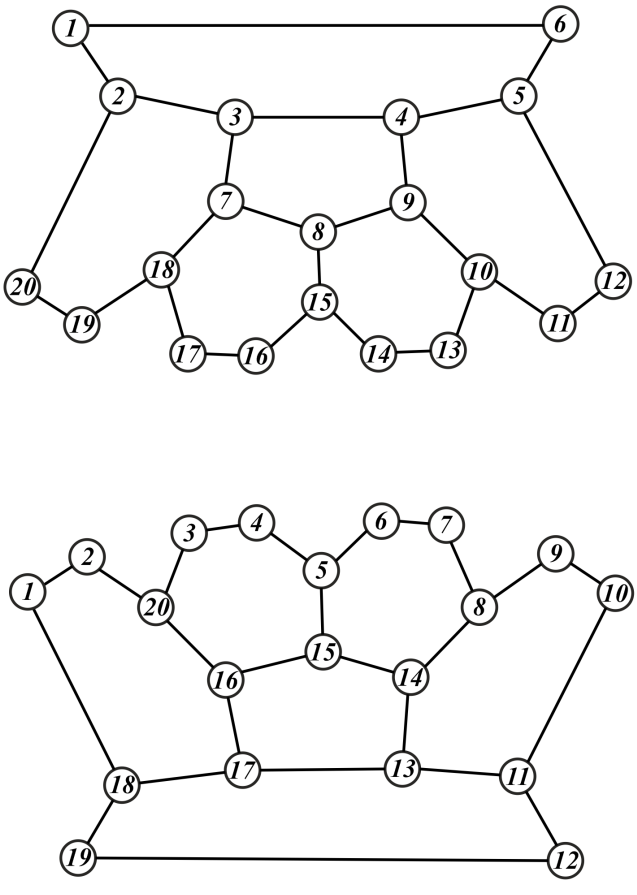

Fig. 4. Schlegel diagram of the $C_{50}Cl_{10}$ compound after the expulsion of nodes with sp^3 hybridization.

Table 1. The energy spectrum of the compound $C_{50}Cl_{10}$ at parameters **U** = 8.1 eV, **B** = −1 eV.

-6.725, 1.0	-3.573, 2.0	1.375, 1.0	4.527, 2.0
-6.145, 2.0	-3.050, 1.0	1.955, 2.0	5.050, 1.0
-5.589, 1.0	-2.836, 1.0	2.511, 1.0	5.264, 1.0
-5.517, 2.0	-2.694, 2.0	2.583, 2.0	5.406, 2.0
-4.827, 2.0	-2.273, 2.0	3.273, 2.0	5.827, 2.0
-4.788, 2.0	-1.583, 2.0	3.312, 2.0	6.517, 2.0

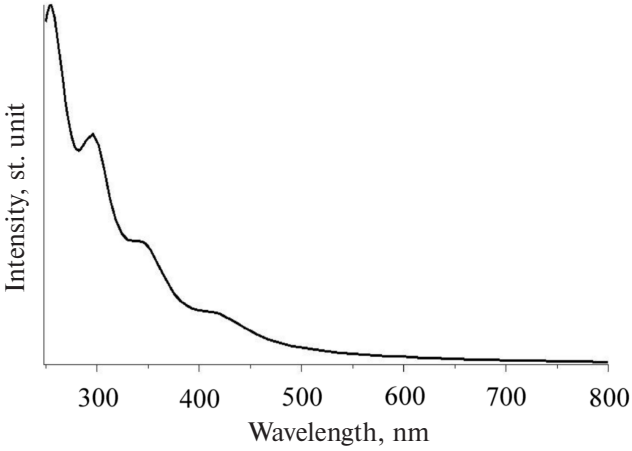

Fig. 5. The theoretical curve of the OAS of the compound $C_{50}Cl_{10}$ obtained in this work.

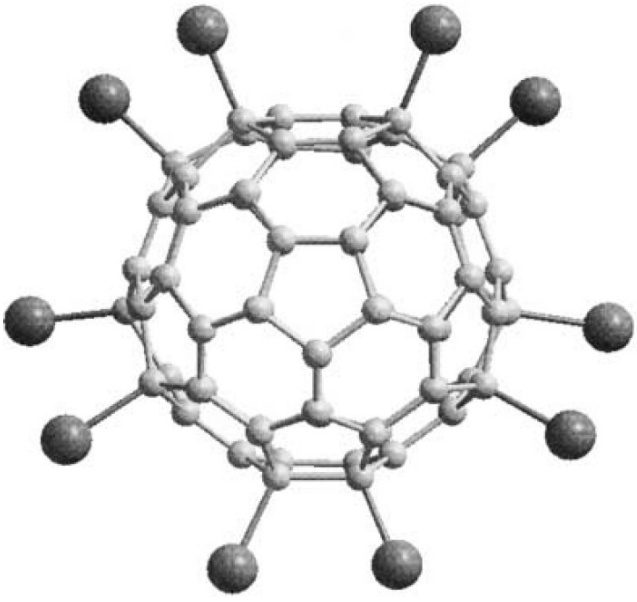

Fig. 6. Image of a $C_{70}Br_{10}$ molecule. View from the "pole". Data from [27] were used.

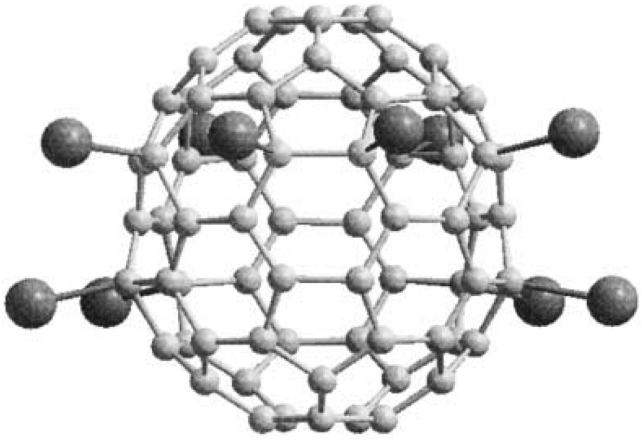

Fig. 7. Image of $C_{70}Br_{10}$ molecule. View from the "equator". Data from [27] were used.

and vacant positions, referred to as the HOMO-LVMO, is about 2.9 eV, the HOMO is an upper filled molecular orbital, and the LVMO lower vacant molecular orbital. The OAS calculated by us in accordance with formula (12) is shown in Fig. 5. It can be seen that on the theoretical curve the absorption edge is the same as on the experimental one, and corresponds to the value of the value of the order 2.9 eV. There are also absorption bands on the curve with maxima at wavelengths of 250, 300 nm, in the region of wavelengths from 320 to 350 nm, there is a plateau, which apparently corresponds to three weakly pronounced maxima at 322, 334, 356 nm.

Thus, the results obtained in the framework of our model and the method described at the beginning of the current work for the $C_{50}Cl_{10}$ compound are in good qualitative agreement with the experimental data of the work [11].

4. THE ENERGY SPECTRUM AND OPTICAL ABSORPTION OF $C_{70}Br_{10}$ COMPOUND

The synthesis of the compound $C_{70}Br_{10}$ was reported in [12]. The synthesis was carried out using C_{70} fullerenes. Fullerene was mixed with some amount of Br_2. After drying the mixture and certain processing, samples of $C_{70}Br_{10}$ with a mass purity of 99% were obtained. Before work [12] at work [27] the structure of this compound was established, the symmetry group to which it belongs turned out to be C_s. Figures 6 and 7 show images of $C_{70}Br_{10}$ molecule were used in two angles, the data were taken from the work [12]. Fig. 8 shows its Schlegel diagram, the data are taken from [27].

Within the framework of the model we use, there is no difference in which chemical element, Br or Cl, participates in the compound, both elements form a bond with the

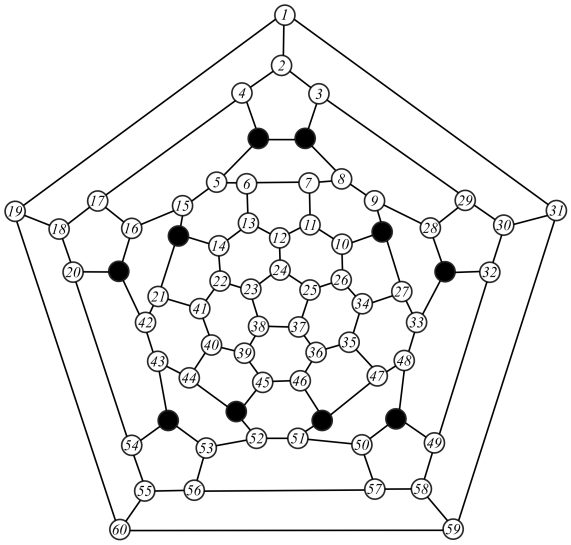

Fig. 8. Schlegel diagram $C_{70}Br_{10}$. The Br atoms are marked with solid circles. The data from the work [27] were used.

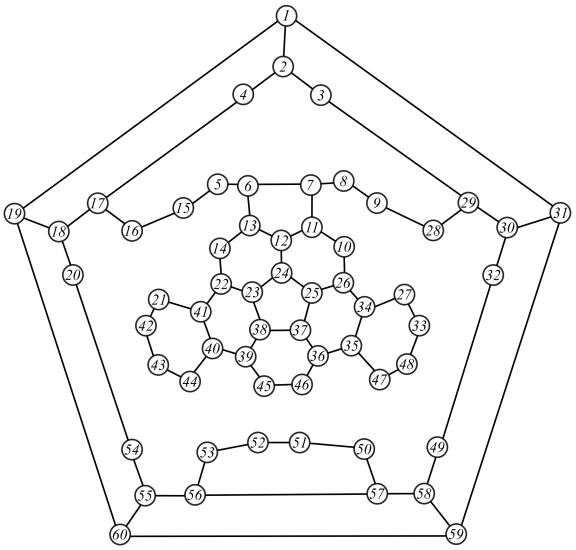

Fig. 9. The Schlegel diagram, depicting only the atoms in the sp^2-state of the $C_{70}Br_{10}$ compound.

carbon atom, as a result, the carbon atom at the point of attachment passes into the sp^3-state. Therefore, to obtain the energy spectrum and the OAS curve, we will use the model used by us in the study of the compound $C_{50}Cl_{10}$. Thus, we will work with the system, the Schlegel diagram of which is shown in Fig. 9, where only those carbon atoms that are in the sp^2-state are left.

The energy spectrum of this system at values of the parameters of the Hubbard model U = 7.15 eV, B = –1.0 eV is shown in table 2. It can be seen that it contains 116 levels, 58 levels in each Hubbard subzone. Among all the levels, two levels, one in each subzone, are doubly degenerated, the rest are not degenerated. The width of each Hubbard subzone is approximately 5.33 eV, and the gap between them is about 1.82 eV.

The OAS curve, calculated in the same way as for the $C_{50}Cl_{10}$ system, is shown in Fig. 10. The experimental OAS curve, obtained on the basis of data from [12], is shown in Fig. 11. It can be seen that in experimental and theoretical curves, there is an absorption band with a maximum at a wavelength of $\lambda \approx 400$ nm. On the theoretical curve there is an absorption band with a wide maximum in the range from 430 nm to 580 nm, on the theoretical one in this area there are two absorption bands, which appear on the curve as two “bulgings”. In our opinion, these two absorption bands correspond to a wide maximum at 500 nm on the experimental curve. On both curves, theoretical and experimental, an absorption boundary is observed at a wavelength of $\lambda \approx 650$–680 nm, approximately corresponding to the gap of

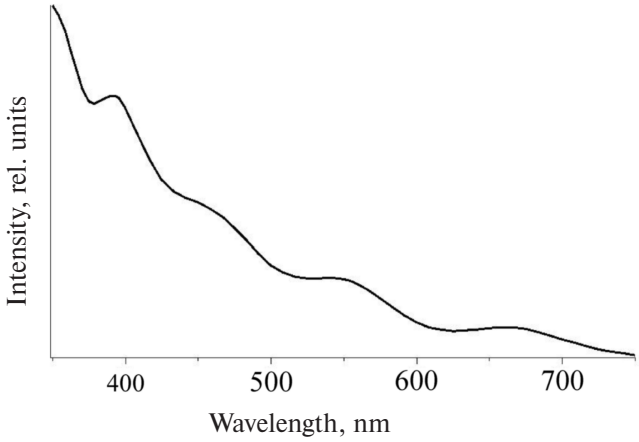

Fig. 10. The $C_{70}Br_{10}$ OAS curve obtained in this work using formula (12) Intensity, rel. units; wavelength, nm.

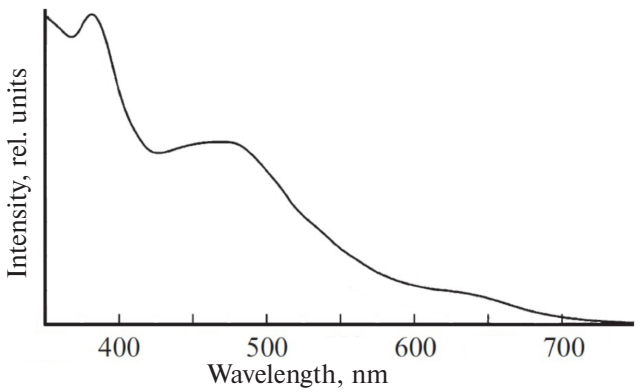

Fig. 11. The $C_{70}Br_{10}$ OAS curve obtained based on data from [12] Intensity, rel. units; wavelength, nm.

the HOMO-LVMO, equal to 1.82 eV. In conclusion, for the $C_{70}Br_{10}$ system, the critical OAS was also obtained using the formula (9), it is shown in Fig. 12.

Table 2. The energy spectrum of the compound C70Br10at parameters U = 7.15 eV, B = –1 eV.

–6.336, 1.0	–3.432, 1.0	0.814, 1.0	3.718, 1.0
–6.293, 1.0	–3.312, 1.0	0.857, 1.0	3.838, 1.0
–5.996, 1.0	–3.021, 1.0	1.154, 1.0	4.129, 1.0
–5.932, 1.0	–3.012, 1.0	1.218, 1.0	4.138, 1.0
–5.882, 1.0	–2.969, 1.0	1.268, 1.0	4.181, 1.0
–5.775, 1.0	–2.790, 1.0	1.375, 1.0	4.360, 1.0
–5.602, 1.0	–2.786, 1.0	1.548, 1.0	4.364, 1.0
–5.500, 1.0	–2.663, 1.0	1.650, 1.0	4.487, 1.0
–5.429, 1.0	–2.575, 2.0	1.721, 1.0	4.575, 2.0
–5.376, 1.0	–2.336, 1.0	1.774, 1.0	4.814, 1.0
–5.309, 1.0	–2.323, 1.0	1.841, 1.0	4.827, 1.0
–5.216, 1.0	–2.289, 1.0	1.934, 1.0	4.861, 1.0
–5.068, 1.0	–2.256, 1.0	2.082, 1.0	4.894, 1.0
–5.009, 1.0	–2.248, 1.0	2.141, 1.0	4.902, 1.0
–4.999, 1.0	–2.243, 1.0	2.151, 1.0	4.907, 1.0
–4.929, 1.0	–2.152, 1.0	2.221, 1.0	4.998, 1.0
–4.925, 1.0	–1.962, 1.0	2.225, 1.0	5.188, 1.0
–4.725, 1.0	–1.875, 1.0	2.425, 1.0	5.275, 1.0
–4.691, 1.0	–1.843, 1.0	2.459, 1.0	5.307, 1.0
–4.575, 2.0	–1.770, 1.0	2.575, 2.0	5.380, 1.0
–4.432, 1.0	–1.730, 1.0	2.718, 1.0	5.420, 1.0
–4.394, 1.0	–1.630, 1.0	2.756, 1.0	5.520, 1.0
–4.382, 1.0	–1.476, 1.0	2.768, 1.0	5.674, 1.0
–4.376, 1.0	–1.417, 1.0	2.774, 1.0	5.733, 1.0
–4.285, 1.0	–1.338, 1.0	2.865, 1.0	5.812, 1.0
–4.263, 1.0	–1.054, 1.0	2.887, 1.0	6.096, 1.0
–4.210, 1.0	–1.018, 1.0	2.940, 1.0	6.132, 1.0
–4.111, 1.0	–1.015, 1.0	3.039, 1.0	6.135, 1.0
–3.792, 1.0	–1.004, 1.0	3.358, 1.0	6.146, 1.0

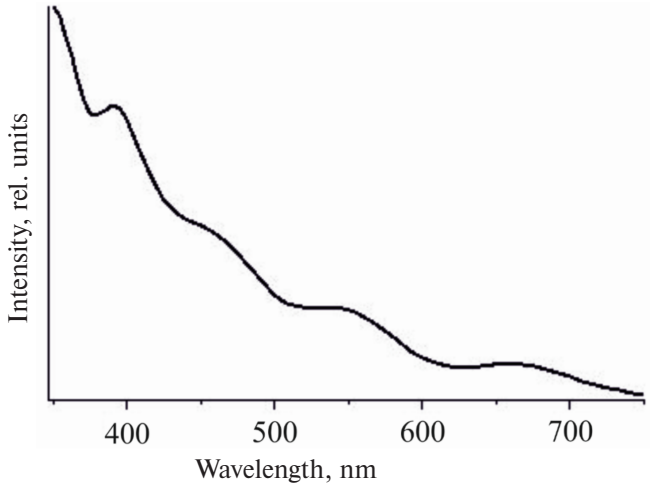

Fig. 12. The $C_{70}Br_{10}$, OAS curve obtained in this work using formula (9).

A comparison of the curves obtained by formulas (9) and (12) presented in Fig. 12 and 10, respectively, shows that they practically do not differ from each other. Based on this, it can be assumed that in systems with low symmetry, for example C_s, both methods of calculating OAS based on formulas (9) and (12) give the same results, due to the fact that in systems with low symmetry we take into account all transitions, and they cannot be divided into "permitted" and "prohibited" ones. This assumption requires a separate study.

5. CONCLUSION

Thus, a theoretical study of the compounds $C_{70}Br_{10}$ and $C_{50}Cl_{10}$ in the framework of the approximation of static fluctuations for the Hubbard model showed that the OAS curves obtained within this approximation are in qualitative agreement with experimental data. This indicates both the applicability of the Hubbard model and the adequacy of the used SFA approximation. In addition, the results of the work also indicate the need to take into account the fact that carbon in the nodes through which the halogen atoms are attached passes from the hybridized sp^2-state to the sp^3-state.

REFERENCES

1. D.V. Konarev, R. N. Lyubovskaya, Advances in Chemistry 81, 336 (2012).
2. Su-Yuan Xie, Fei Gao, Xin Lu et al., Science 304, 699 (2004).
3. A.I. Murzashev, JETP, 135, 122 (2009).
4. G.I. Mironov, A. I. Murzashev, FTT,– 2011, 53, 2273 (2011).

5. T.E. Arutyunova, G. I. Mironov, A. I. Murzashev, FTT, 54, 1797 (2012). 13
6. A.I. Murzashev, A. P. Zhumanazarov, I. E. Kareev, et al., FTT, 65, 344 (2023).
7. A.I. Murzashev, N. V. Melnikova, A. P. Zhumanazarov et al., Optics and spectroscopy, 131, 691 (2023).
8. A.I. Murzashev, FTT, 62, 484 (2020).
9. A.I. Murzashev, T. E. Nazarova, JETP, 146, 1026 (2014).
10. A.I. Murzashev, E. O. Shadrin, JETP, 145, 1161 (2014).
11. Jian-Hua Chen, Zhi-Yong Gao, Qun-Hong Weng et al., Chem. Eur. J., 18, 3408 (2012).
12. K.N. Semenov, N. A. Charykov, A. S. Kritchenkov, J. Chem. Eng. Data 58, 570 (2013).
13. A.V. Silantiev, FTT, 64, 750 (2022).
14. A.V. Silantiev, FTT, 65, 157 (2023).
15. A.A. Levin, Introduction to quantum chemistry of solids. M.: Chemistry, 1974. 237 p.
16. T.O. Wehling, E. ¸Sa¸sıo˘glu, C. Friedrich, et al., Phys. Rew. Lett.106, 236805 (2011).
17. J. Hubbard, Proceedings of the Royal Society, 276, 238 (1963).
18. P.R. Wallace, Phys. Rew., 71, 622 (1947).
19. G.I. Mironov, FMM, 102, 611 (2006).
20. A.A. Abrikosov, Fundamentals of the theory of metals, Science, Moscow (1987), 521 p.
21. R.O. Zaitsev. Diagram methods in the theory of superconductivity and ferromagnetism, "Editorial URSS", Moscow (2010), 175 p.
22. L.D. Landau, E. M. Lifshitz, Quantum Mechanics, Science, Moscow (1989), 768 p.
23. A.I. Murzashev, A. P. Zhumanazarov, M. Yu. Kokurin, Optics and spectroscopy. 129, 1111 (2021).
24. A.I. Murzashev, A. P. Zhumanazarov, M. Yu. Kokurin, etc. Optics and spectroscopy, 130, 979 (2022).
25. A.A. Abrikosov, L. P. Gorkov, I. E. Dzyaloshinsky, Methods of quantum field theory in statistical physics. Fizmatgiz, Moscow (1962), 444 p.
26. I.E. Kareev, V. P. Bubnov, A. I. Kotov et al. FTT, 59, 200 (2017).
27. S.I. Troyanov, A. A. Popov, N. I. Denisenko et al., Chem. Int. Ed., 42, 2395 (2003).